PCCP

Accepted Manuscript

ROYAL SOCIETY OF CHEMISTRY

www.rsc.org/pccp

Journal Name

ARTICLE TYPE

Cite this: DOI: 10.1039/xxxxxxxxxx

Disk to Dual Ring Deposition Transformation in Evaporating Nanofluid Droplets from Substrate Cooling to Heating†

Xin Zhong,[a] and Fei Duan,[a,*]

Received Date
Accepted Date

DOI: 10.1039/xxxxxxxxxx

www.rsc.org/journalname

The substrate temperature plays an important role in the deposited morphologies formed after the evaporation of nanofluid droplets. The deposited patterns are shown to vary from a uniform disk-like profile to a dual ring from cooling to heating of the substrate. The droplet on the substrate with a relatively low temperature reveals three primary stages. Stage I features an outward transport of nanoparticles along the liquid-air interface near the droplet edge. Meanwhile some nanoparticles form sediment on the solid surface with a certain distance to the contact line. In the central region nanoparticles are dominated by Brownian motion so they fluctuate around their positions. Stage II is characterized by an increasing outward travelling of nanoparticles in the bulk so the coffee ring is gradually enhanced. Most particles in Stages I and II are central-concentrated, leaving an annular gap sparsely covered adjacent to the outer ring. In Stage III, the pattern is homogenized by filling the gap with the arrival of the interior nanoparticles. Upon increasing the substrate temperature, the accompanied flow pattern exhibits a transition when the substrate still stays cooler than the atmosphere. It is resulted from the evaporative cooling at the droplet apex counteractive to the applied temperature gradient by substrate cooling. Above the transition temperature, the induced inward Marangoni flow is brought in advance at a higher substrate temperature, and in conjunction with the outward radial flow a dual ring pattern is formed.

1 Introduction

Particle deposition from evaporating suspension droplets has been extensively investigated propelled by both scientific exploration and industrial applications across the fields of manufacturing, biology, medical science, etc. From the pioneering effort of probing the ubiquitous coffee ring effect by Deegan, et al.[1] to the countless attempts aiming to manipulate the solutes morphology, understanding of colloidal droplet evaporation has been greatly promoted from the aspects of wettability control[2], contact line dynamics[3], flow paradigms[4], interactions among particles with the solid and liquid phases[5], particles assembly[6], etc. Corresponding strategies in a variety have been proposed to manipulate the aspects of the base solution[7–15], the suspended solutes[16–24], the solid substrates[25–29], and the external interventions for droplet evaporation[30–32].

The effect of solid substrates has been reported to vary the flow patterns owing to the induced temperature gradients of the sessile droplets. The greatest evaporation at droplet edge correlated with the decreased droplet thickness along the radius could result in a heterogeneous temperature profile along the liquid-air interface[33,34]. Ristenpart, et al.[35] proposed a quantitative criterion based on the relative thermal conductivities of the substrate to the liquid, k_r, to determine the direction of the thermal Marangoni flow along the droplet surface. The evaporative cooling at droplet rim is normally neglected when k_r is large, since for substrates with high conductivities energy can be provided instantly to the contact line region for mainly replenishing the heat loss resulting from phase change. This study of Ristenpart, et al.[35] implies the role of substrate properties in defining the flow pattern of sessile drops. Xu, et al.[36] further pointed out the dependence of the Marangoni flow direction on the ratio of the substrate thickness to the droplet contact radius. Apart from droplet evaporation taking place at room temperature, substrate heating has also drawn more attention. Parsa, et al.[25] showed that the deposit evolved from a uniform distribution to a dual ring and then a stick-slip pattern upon increasing the substrate temperature. The temperature gradient detected by an infrared technique was shown to orient to the contact line for both the natural and heating conditions, in consistent to the

[a] School of Mechanical and Aerospace Engineering, Nanyang Technological University, 50 Nanyang Avenue, Singapore 639798, Singapore. E-mail: feiduan@ntu.edu.sg

† Electronic Supplementary Information (ESI) available: A period of Stage I (ES1), Stage II (ES2) and Stage III (ES3) of the droplet on the 10 °C substrate. ES4 shows the nanoparticles reversal at the free surface of the droplet on the 20 °C substrate. See DOI: 10.1039/b000000x/

temperature profiles obtained by Girard, et al.[37]. Subjected to the same mechanism that the inward Marangoni flow is enhanced upon heating the solid surface, the deposited profile transferred from a single ring to a dual ring formed by polystyrene spheres in the study of Li, et al.[26].

Despite plenty of the studies stressing on natural and heating conditions, the effect of substrate cooling on evaporating sessile droplet containing suspensions is rarely examined. To our knowledge, only Kim, et al. obtained the solutes distribution from evaporating droplets on substrates cooled down to utmost 22 °C[38]. The central-concentrated deposit under substrate cooling altered to a ring-shaped stain with heating the substrate. The evolution of the local solute concentration was probed by a technique of light absorbance. Here we report an experimental study addressing the influence of substrate temperature from cooling to heating on the evaporation of sessile nanofluid droplets reflected by direct visualizations of nanoparticles movement throughout the droplet lifetime. The deposited profile is more uniform at a lower substrate temperature, and it transfers to a dual ring as the substrate is heated up. The transition for both the flow pattern and the deposited profile, to our surprise, emerges when the substrate is controlled still cooler than the atmosphere. The strong dependence of the deposited profile on the substrate temperature points toward a promising strategy for a robust control of colloids distribution from evaporating suspensions.

2 Experimental Methods

2.1 Materials and Nanofluid Preparation

The nanofluid samples with the nanoparticle concentration at 0.5 g/L were prepared by mixing graphite nanopowders (2-3 nm, SkySpring Nanomaterial Inc., Purity≥99%) and Milli-Q nano-filtered water with resistivity at 18.2MΩ-cm obeying the two-step method. The sample was placed in an ultrasonic bath (Fisher Scientific model 500) at first and then underwent magnetic stirring to obtain evenly dispersed suspensions. The freshly prepared sample was employed within two days to avoid particle agglomeration and sedimentation. The evaporation substrates were brand new silicon wafers (Latech Scientific Supply Pte. Ltd.,) with an average roughness at 0.106μm. The wafers were ultrasonically cleaned in water for 1 hour and then dried by compressed dry nitrogen prior to each test.

2.2 Experimental Setup and Characterization

The experimental configuration is shown in Figure 1. Nanofluid droplet with an initial volume at around 0.2 μL controlled by a micropipette (Thermo-Fisher) was deposited inside a shielding plastic cylinder with open sides on a silicon wafer to avoid external air disturbance. The wafer was attached to the lower aluminum heating module by a thin layer of conductive silica-gel. The heating/cooling bath (F25-EH, JULABO) connected to the heating module controlled its temperature and so was that of the silicon wafer. The silicon wafer temperature is adjusted to 10 °C, 12 °C, 15 °C, 16 °C, 22 °C (room temperature) and 50 °C. Two calibrated K-type thermocouples with the accuracy at 0.1 K were adhered to the surface of the silicon wafer with one at the edge and the other at the center to monitor the temperature uniformity by a Data Acquisition (Agilent, 34972A). The substrate temperature difference from the two thermocouples was less than 0.2 K during the entire droplet lifetime thanks to the high conductivity of the silicon wafer.

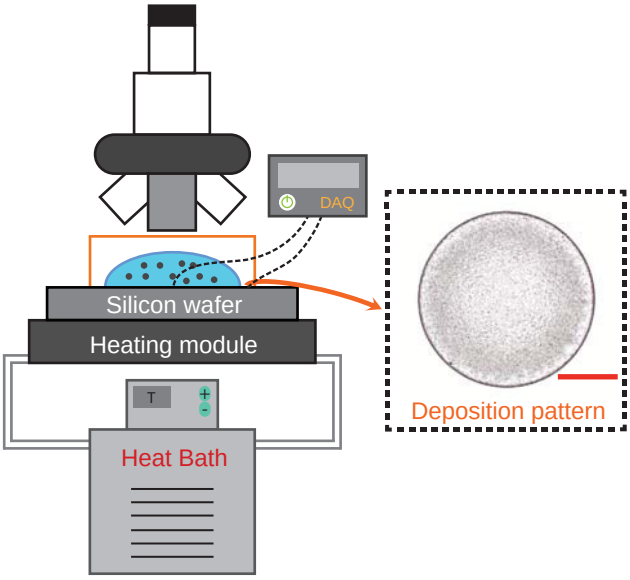

Fig. 1 (Color online) Schematic diagram of the experimental configuration consists of an optical microscope visualizing the droplet placed on the silicon wafer substrate which is adhered to the heating alumina module below. The module temperature is controlled by the heating/cooling bath. Two thermal-couples are attached to the silicon wafer with one at the center and the other at the edge to monitor the substrate temperature by a Data Acquisition (DAQ). After droplet evaporation, a deposition pattern is left on the substrate as shown by the image at the right side. The scale bar indicates 400 μm.

We employed an optical microscopy (LV100D-U from Nikon Inc.) with bright-field (BF) and dark-field (DF) schemas to obtain particles motion during droplet evaporation and the resulting nanoparticles profiles from a top view. The time 0 s is defined as the moment when the droplet touches the substrate. In order to probe nanoparticle motion along the cross-section of the droplet, the microscope was adjusted to focus at either the solid-liquid or the liquid-air interfaces. Whether a particle or an aggregate is at focus suggests us its approximate vertical position. After droplet evaporation completed, the “three-dimensional light intensity analysis" and the “inverted grayscale intensity analysis" of the microscope were utilized to present the spatial and the radial stain distribution for the droplets respectively. At least three batches of tests were conducted for each substrate temperature to guarantee experimental repeatability. The experiments were conducted under the ambient condition with the temperature and the relative humidity fixed to 22 °C and 40%∼50%.

3 Results and Discussion

3.1 Deposited Profiles at Various Substrate Temperatures

The particle deposition profiles are shown in Figure 2 at each substrate temperature. The pattern is displayed from a top view together with its “three-dimensional light intensity profile" and

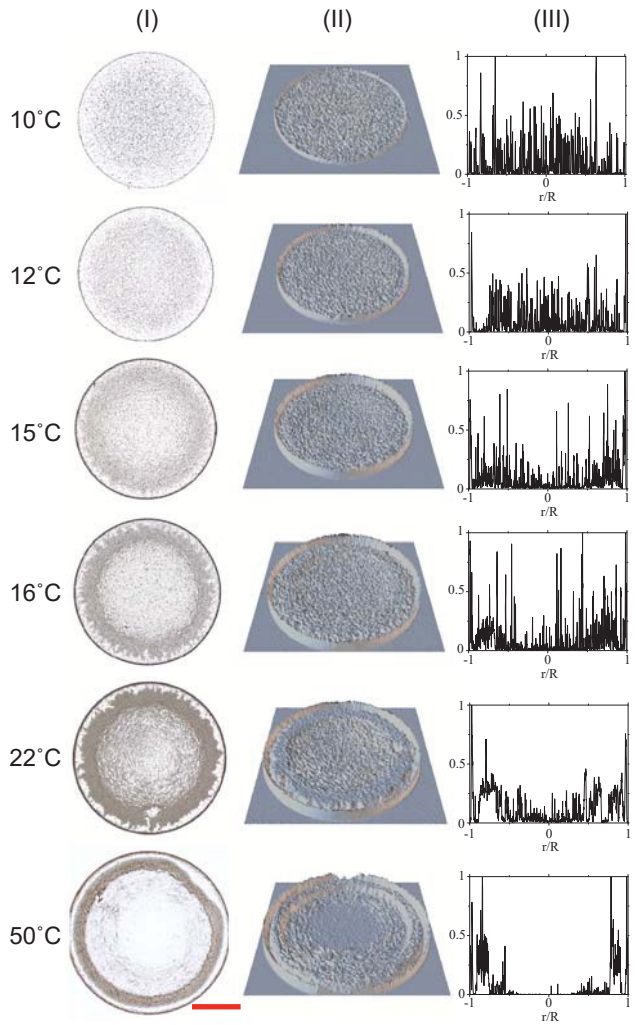

Fig. 2 (I) The deposition patterns, (II) the corresponding three-dimensional light intensity profiles and (III) the normalized inverted grayscale intensity profiles along the diameter from the 0.5 g/L graphite nanofluid droplets on the silicon wafer substrates with the surface temperature at 10 °C, 12 °C, 15 °C, 16 °C, 22 °C and 50 °C. The scale bar indicates 400 μm.

the "normalized inverted grayscale intensity profile" reflecting the spacial and radial nanoparticles distributions. At 10 °C, a disk-like deposition is produced with nanoparticles uniformly covering the interior region enclosed by an exterior coffee ring, except for a fairly narrow annular gap adjacent to the edge where the nanoparticles are more sparsely distributed. At 12 °C and 15 °C, the coverage of the nanoparticles at the annular gap is further reduced, and at 16 °C there barely has nanoparticles. Meanwhile, contrary to the uniform central region at 10 °C, the interior deposit becomes hollow with the increase of the substrate temperature. The vacancy detectable at 12 °C and 15 °C becomes evident at 16 °C. As the temperature reaches 22 °C and 50 °C, the interior deposition has entirely alters to a secondary ring.

Figure 2 reveals that the deposited profile transfers from a homogeneous pattern to a dual ring with an increase of the substrate temperature, and the transit point seems to occur at around 15 °C to 16 °C when the secondary ring begins to take shape while the central region is still uniformly covered with nanoparticles. After carefully examining the nanoparticles motion upon droplet evaporation, it is strikingly found that the flow paradigm is distinctly different for the substrate below and above roughly 16 °C. Therefore, we decompose the phenomena for the two corresponding temperature ranges.

3.2 Flow Patterns under Substrate Cooling at 10 °C

Droplets placed on the cooler substrates were found to display evolving fluid flow patterns with the proceeding of evaporation instead of a mono-paradigm. The droplet on the 10 °C substrate exhibited three evaporation stages which were distinguished by the distinct nanoparticle trajectories in each stage along the liquid-air interface, near the solid surface or in the bulk. The intensity and duration of each stage were greatly affected by the substrate temperature, and the combination of the stages determined nanoparticles locations and the deposit profile as a whole.

At the moment the droplet was placed on the substrate cooler than the surrounding atmosphere, the droplet edge was cooled down firstly, and the surface temperature should increase as going away from the perimeter. Therefore, the surface tension near the droplet perimeter is higher, so the nanoparticles at the liquid-air interface are carried towards the contact line. It was evidenced by the outward motion of the nanoparticle aggregates shown in the frames of Figure 3 (a). The aggregates denoted by the yellow and the red circles are vaguely observed at time 8.2 s as the microscope focuses at the solid-air interface, suggesting that they are nearer to the liquid-air interface. At 151 s the aggregates carried to approach the contact line region are clearly visualized by the microscope. The enhancement in the clarity of these aggregates confirms their trajectories along the droplet free surface. Meanwhile, at the liquid-air interface far away from the contact line, nanoparticles were observed to fluctuate erratically around their original positions, implying the domination of Brownian motion. Simultaneously, a few nanoparticles close to the solid surface are shown to directly rest on the substrate without evident horizontal displacements. It suggests that there has no advective flow or that such a flow is too weak to induce massive transports of nanoparticles no matter inwards or outwards. The aggregates denoted by the number "1", "2", "3" or "4" at time 8.2 s are away from the solid surface according to their blurring outlines. While at 57.1 s, the four aggregates can be observed clearly, implying that they have descended onto the substrate. Besides, it is found that the four aggregates barely change their horizontal locations before and after the sedimentation. The motion of the nanoparticles in Stage I is also shown in the Supporting Information (Video ES1).

We noticed that nanoparticles were seem to be repelled from reaching the annular region neighboring the contact line in this stage despite that there had no perceptible inward motion of nanoparticles observed in our experiment. It differs from the flow pattern proposed by Kim, et al.[38] that the temperature gradient induced outward Marangoni flow along the liquid-air

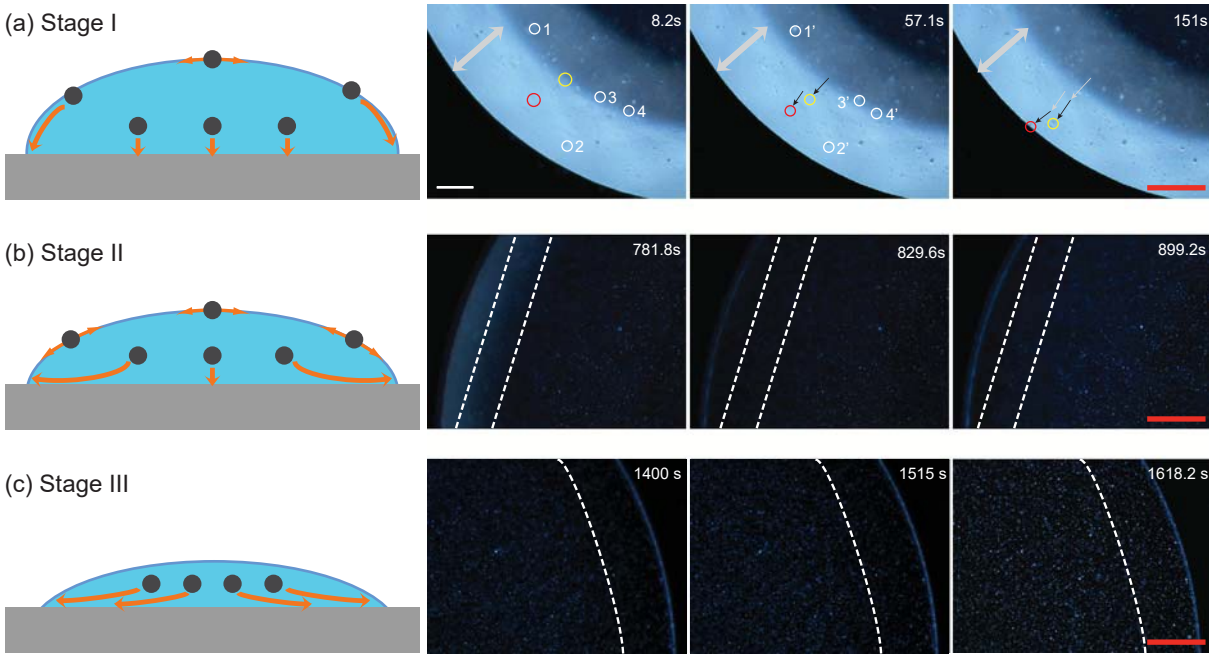

Fig. 3 (Color online) The entire evaporation of the droplet placed on the 10 °C substrate is divided into (a) Stage I, (b) Stage (II) and (c) Stage (III) with the corresponding schematic diagram at the left. For Stage I, the snapshots taken at 8.2 s, 57.1 s and 151 s indicate the outward transport of two nanoparticle aggregates along the liquid-air interface denoted by the red and the yellow circles, and the descendence of the four aggregates onto the solid surface denoted by the number "1", "2", "3" or "4". The arrows denote an annular gap with sparsely-distributed nanoparticles next to the contact line. In Stage II, the snapshots taken at 781.8 s, 829.6 s and 899.2 s at the right side show some nanoparticles under Brownian motion at the liquid-air interface without palpable orientations. In Stage III, the snapshots at 1400 s, 1515 s and 1618.2 s indicate the filling of the annular gap adjacent to the contact line by outward transported nanoparticles. The scale bar indicates 100 μm.

interface triggered an inward flow near the solid surface which brought dissolved polymers to the central area, evidenced by the evolution of the light absorbance there. The discrepancy between the study from Kim, et al. and ours could be attributed to the weaker droplet wettability in their study such that the larger droplet thickness and contact angle were likely to enhance the temperature gradient and thus the accompanied inward flow near the substrate. This could also account for the more central-concentrated deposit profile even at a smaller temperature difference between the atmosphere and the substrate in their study. The absence of an outward radial flow should be partially accountable to the annual vacant gap adjacent to the coffee ring shown in Figure 2 (a).

Stage I lasted for roughly a short 15% of the droplet lifetime for the 10 °C substrate. Its ending is characterized by an increase of the nanoparticles in the bulk driven radially outward so the coffee ring is gradually pronounced, as indicated by the snapshots in panel (b) of Figure 3. Besides, the outward transport of nanoparticles along the liquid-air interface is remarkably attenuated and instead they randomly oscillate without a palpable trend. The snapshots in panel (b) of Figure 3 taken from Video ES2 demonstrate some nanoparticles at the droplet free surface between the two dashed lines fluctuating locally over even 100 s. The absence of the outward transport of nanoparticles along the liquid-air interface was attributed to the homogenized temperature profile of the droplet due to a longer time of cooling. In addition, the nanoparticles at the central region near the solid surface were less affected by the enhanced radial flow, and they still descended toward the solid surface directly. The behaviors of the nanoparticles at the liquid-air, the liquid-solid interfaces and in the bulk are schematized at the left side of Figure 3 (b). The droplet kept pinned during Stage II so the height decreased due to by evaporation. The associated evaporation flux and the radial advective flow were enhanced, carrying plenty of nanoparticles to contribute to the coffee ring. Even though the outward transports of the nanoparticles in the bulk solution were enhanced, the annual gap next to the contact line still remained sparsely-covered. The low temperature at 10 °C of the substrate allowed a relatively slow evaporation, so the outward flow with an intermediate velocity enabled the nanoparticles to arrive at the contact line region and freely assembled with the coffee ring, rather than being flushed to hit the annual vacant area before reaching the droplet edge.

Stage III represents the instantaneous dry-up of the droplet at the latest moment (Figure 3 (c) and Video ES3). The annular region confined by the coffee ring and the dashed curve has few nanoparticles as shown by the image taken at 1400 s in panel (c) of Figure 3. But as the radial capillary flow increases greatly at the ultimate stage, nanoparticles and their congregates are flushed outwards to fill the vacant annular region, as shown by the frames at 1515 s and 1618.2 s in Figure 3 (c). In Stages I and II, along with the downward liquid-air interface, some nanoparticles deposited onto the substrate due to the lack of evident flows in the bulk. Therefore, before the droplet dried out, the central region had been already covered with plenty nanoparticles. They could block the free pathes of those close to the substrate, and allow

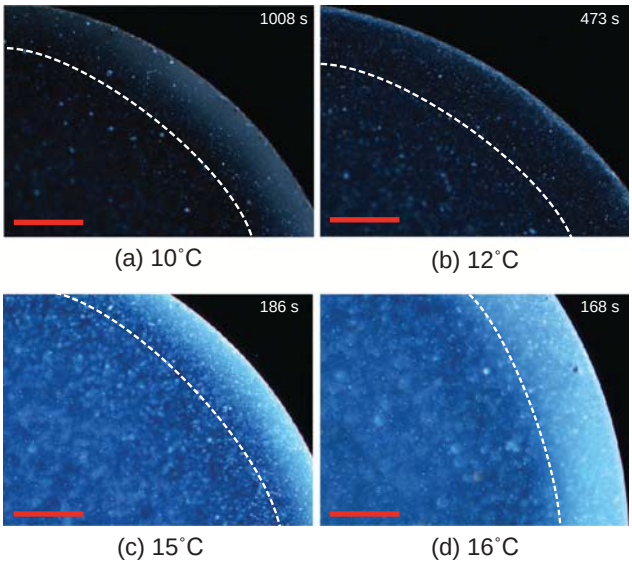

Fig. 4 (Color online) The snapshots taken at around 50% of the lifetime of the 0.5 g/L graphite nanofluid droplet on the (a) 10 °C, (b)12 °C, (c)15 °C and 16 °C substrates. The region confined by the dashed curve and the contact line is sparsely covered at the 10 °C and 12 °C substrates, while it is densely covered at the 15 °C and 16 °C substrates. The scale bar indicates 100 μm.

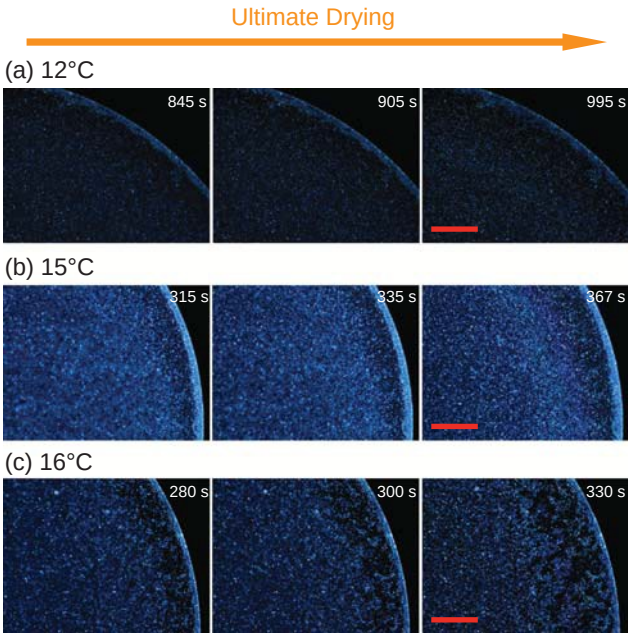

Fig. 5 (Color online) Snapshots of the ultimate drying of the 0.5 g/L graphite nanofluid droplets on the (a) 12 °C, (b) 15 °C and (c)16 °C substrates. The scale bar indicates 100 μm.

them to transport only by a short distance before immobilized. It explains why many nanoparticles ended with touching the previous vacant annular area near the perimeter, resulting in a homogenized morphology for the entire droplet region.

3.3 Flow Patterns upon Increasing the Substrate Temperature from 10 °C to 16 °C

The pattern evolving from a homogenous profile to a blurring dual ring from 10 °C to 16 °C of the substrate was determined by the combination of the three stages. The duration, intensity and even nanoparticles transport for each stage were sensitive to the substrate temperature. It is worth mentioning herein that as the substrate temperature increased, the transition from Stage I to II was difficult to distinguish since even at an early moment a few nanoparticles were noticed to be carried outward in the bulk, particularly at 15 °C and 16 °C. One thing can be seen is that Stage I was conspicuously shortened and the onset of Stage II was brought in advance with a raise of the substrate temperature. Although at the very beginning the particles directly resting on the solid surface were still observable, the amount of which was substantially reduced. Most nanoparticles in the bulk were dominated by the enhanced outward flow owing to the intensified evaporation at a higher substrate temperature. Their relatively high velocity resulted in a greater chance of their impact on the annular region. The snapshots taken at the same time of 50% of each droplet lifetime in Figure 4 present that from 10 °C to 16 °C, the region confined by the contact line and the dashed curve is more densely distributed at a higher temperature. The massive outward transport of the nanoparticles was expected to reduce the amount of them remaining in the central bulk, which thinned the central deposit and thus the hollowing there was enhanced upon increasing the substrate temperature.

Other two essential reasons for the deposit variation is that in Stage III the amount of nanoparticles capable of reaching the annular vacant region is reduced and that nanoparticle aggregates trapped at the liquid-air interface reverse their directions. At 10 °C of the substrate, nanoparticles are monotonously driven outward to fill the annular gap right before drying out, as shown by the snapshots in Figure 3 (c). Such a phenomenon manifests itself as well in the droplet at the 12 °C substrate (see Figure 5(a)). The annular vacancy at time 845 s is partially covered by the outward swept nanoparticles despite of a thin region remaining uncovered next to the coffee ring. It is worth noticing that the outward transported nanoparticles in Stage III which can reach the vacant region formed in Stages I and II are substantially reduced when the substrate temperature is elevated. Therefore, the vacant region is more obvious with increasing the substrate temperature. At 15 °C, particles carried to the gap are further reduced, and the gap is even slightly extended from 315 s to the end of evaporation (Figure 5 (b)). For the droplet at 16 °C, the aggregates at the liquid-air reverse their orientations distinctly to depart away from the contact line (Figure 5 (c)). Consequently, the gap is widened and it further enhances the secondary ring. Therefore, it can be concluded that lowering the substrate temperature actually suppressed the inward transports of nanoparticles at the liquid-air interface. Additionally, right before droplet drying out, the thin droplet thickness comparable to the size of nanoparticle aggregate made the secondary ring block the free pathes of the nanoparticles travelling outward from the center, which in turn intensified the secondary ring from its inside.

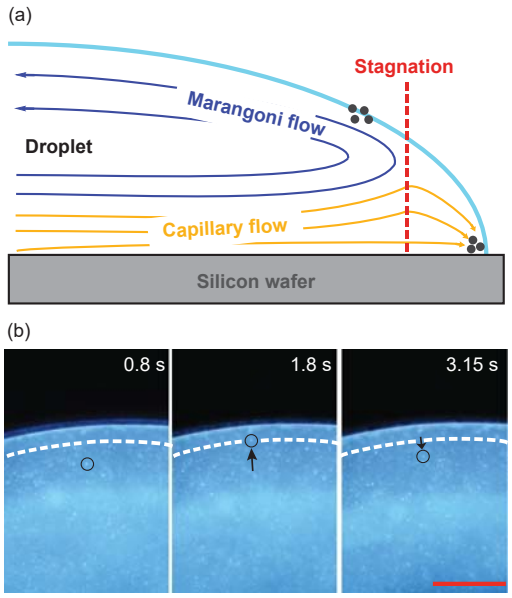

Fig. 6 (Color inline) (a) Sketch of the flow pattern of the co-existing of a Marangoni flow and a radial flow at the substrate temperature higher than 16 °C, with a stagnation point at a distance from the contact line. (b) Snapshots indicate a reversal motion of an aggregate denoted by the circle subject to the Marangoni flow. The dashed curves indicate the position the stagnation point. The scale bar indicates 100 μm.

3.4 Transition of the Flow Patterns and the Deposited Profiles

The flow pattern of the droplet altered greatly as the substrate temperature increased to 16 °C, rather than the room temperature of 22 °C as anticipated. The transition of the flow pattern was mainly embodied in the remarkably intensified outward radial flow, and most importantly the reversal of the surface flow at the latter drying stage. The reversal of the nanoparticle aggregates occurs at the latest moment of droplet drying at the 16 °C substrate (Figure 5(c)), and it gives rise to a discernable inner ring. Such inward nanoparticle transport is brought forward to approximately 57% of the droplet lifetime when the substrate temperature is increased to 20 °C. The corresponding video can be found in the Supporting Information (Video ES4). Despite that the substrate at 16 °C and 20 °C was maintained cooler than the room temperature, the corresponding flow patterns resembled the one at the room temperature and even higher temperatures of the substrate. The water-based droplet evaporating on a silicon substrate at the room temperature was warmest at its edge while coolest at its apex, as reported by Parsa, et al.[25]. Evaporative cooling was greatest at the droplet apex due to the highest resistance to heat conduction from the solid surface. The high relative thermal conductivities of the silicon substrate and the water-based solution enabled energy to be readily supplied to the contact line region, so evaporative cooling would not be produced there[35]. Substrate cooling could counteract the evaporative cooling induced temperature gradient, and even reverse it if the substrate is cooled down to relatively low temperatures. It explained why the inward transport of nanoparticles at the liquid-air interface was still in presence at the 20 °C and 16 °C substrates, while it basically disappeared as the substrate temperature was further lowered.

As the substrate is under natural and heating conditions, the inward motion of nanoparticles along the liquid-air interface emerged at the very beginning of evaporation. Figure 6 (a) shows a schematic drawing of the flow pattern with the co-existing radial flow due to the greater evaporation at the droplet edge and the Marangoni flow induced by a temperature gradient for the substrate temperature equaling and higher than 16 °C in our experiments. The capillary flow leads to the exterior coffee ring while the Marangoni flow brings nanoparticles backwards to accumulate as the inner ring with a certain distance from the contact line. Besides, the stagnation point is found close to the droplet edge, reflected by the reversal of an aggregate firstly carried outwards until arriving at the stagnation point at 1.8 s and then brought back along the liquid-air interface as the substrate is heated to 50 °C (Figure 6 (b)). Many other nanoparticles behave similarly that they reverse the orientations at the stagnation point. It can be seen that the region is free of any nanoparticles beyond the stagnation point indicated by the dashed curve in Figure 6 (b) to the contact line.

Under natural and heating conditions, at the early period nanoparticles were driven radially outward firstly and then were carried to the liquid-air interface near the droplet rim by Marangoni flows. Afterward, the gathered nanoparticles there began to move inwards, forming a distinct secondary ring. Therefore, we decomposed the entire process into two stages, with Stage I featuring the radially outward traveling and the assembling of nanoparticles at the liquid-air interface, and Stage II characterized by the detachment of the annular agglomeration from the contact line to be the inner ring As a comparison, snapshots demonstrating the entire evolutions of the droplets from a top view on the substrates at 10 °C and the room temperature are shown in the panels (a) and (b) of Figure 7 respectively. When the droplet is evaporated on the cooler substrate, the nanoparticles stay in the interior region with an annular gap next to the contact line over Stages I and II. At Stage III, the gap is rapidly filled due to a sudden enhanced outward transport of nanoparticles (Figure 7 (a)). Contrarily, at the room temperature substrate, nanoparticles in the bulk in Stage I are driven outward, emptying the interior region of the droplet. Meanwhile, nanoparticles arrival at the liquid-air interface by Marangoni flows leads to a dense gathering as shown by the frame at 152 s in Figure 7 (b). The dense accumulation of nanoparticle is pulled inside during Stage III and the central hollow is further pronounced, producing a distinct secondary ring at the end of drying. Therefore, it was the combination of the temperature-dependent distinct stages decided nanoparticles transport both at the interfaces and in the bulk, and the last stage was vital for the deposit transition as the substrate was varied from cooling to heating.

4 Conclusions

We experimentally investigated the effect of the substrate temperature from cooling to heating on the flow patterns and the deposited profiles of nanoparticles from the evaporating

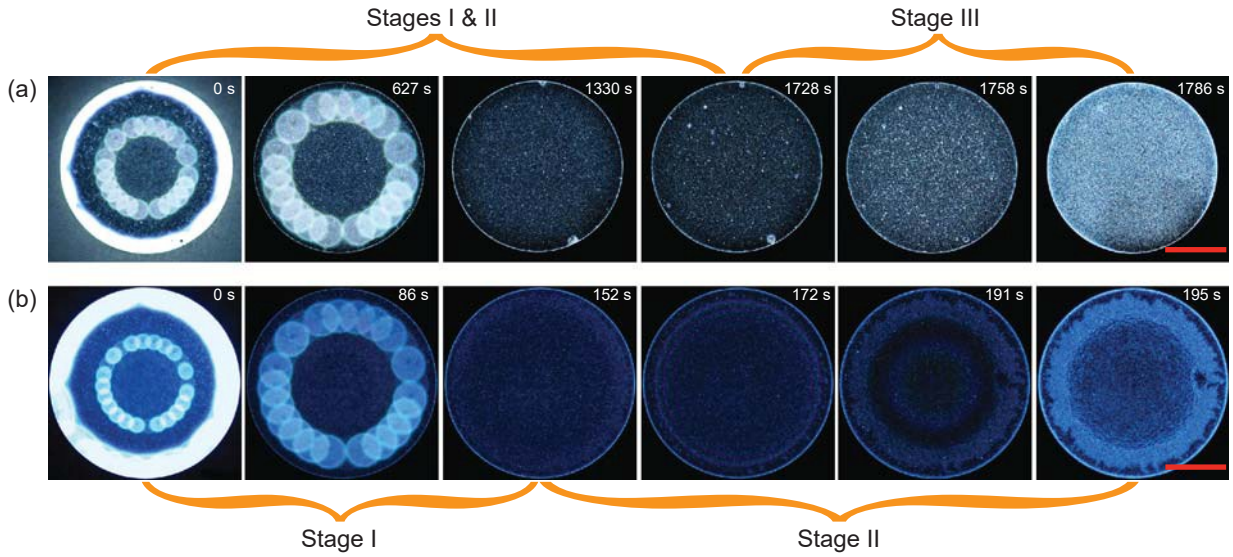

Fig. 7 (Color online) The evaporation process of the 0.5 g/L graphite nanofluid droplet evaporating on the (a) 10 °C and (b) 22 °C substrate. For the droplet on the (a) 10 °C substrate, nanoparticles are central-concentrated with an annular gap next to the contact line during Stages I and II; afterward the gap is filled in Stage III. For the droplet on the 22 °C substrate, nanoparticles are edge-concentrated and lead to a central hollow profile in Stage I; in Stage II the hollow is further enhanced, while the nanoparticle aggregates are transported away from the contact line and form the secondary ring. The scale bar indicates 400 μm.

sessile nanofluid droplets. The deposited patterns transferred from a disk profile to a dual ring with an increase of the substrate temperature. The associated transition of the flow pattern occurred when the substrate was still cooled owing to the counteractive evaporative cooling at the droplet apex. The droplet on the substrate with relatively low temperatures experienced three main stages. In the former two stages most nanoparticles either stayed at the interior region or contributed to the exterior coffee ring, leaving an annular gap between them. And in the last one the pattern was homogenized by filling of the gap by the nanoparticles transported from the interior area. Above the transition temperature of the substrate, the occurrence of the inward Marangoni flow was brought in advance for a higher substrate temperature such that an increasing amount of nanoparticles were carried to the liquid-air interface. Together with the greatly enhanced radial flow which drove the nanoparticles to the contact line, a dual ring pattern was produced after the droplet dried out. Our study highlights the role of substrate temperature in tuning the deposit profiles from suspension droplets, and provides potential for enhancing the deposit uniformity by substrate cooling.

Acknowledgement

The authors acknowledge the support of MOE AcRF Tier 1 (RG120/14).

References

1 R. D. Deegan, O. Bakajin, T. F. Dupont, G. Huber, S. R. Nagel and T. A. Witten, *Nature*, 1997, **389**, 827-829.
2 F. Yang and Y. P. Zhao, *J. Phys. Chem. C*, 2014, **118**, 26859-26865.
3 M. Oksuz and H. Y. Erbil, *J. Phys. Chem. C*, 2014, **118**, 9228-9238.
4 H. Hu and R. G. Larson, *Langmuir*, 2005, **21**, 3972-3980.
5 R. Bhardwaj, X. Fang, P. Somasundaran and D. Attinger, *Langmuir*, 2010, **26**, 7833-7842.
6 Á. G. Marín, H. Gelderblom, D. Lohse, and J. H. Snoeijer, *Phys. Rev. Lett.*, 2011, **104**, 085502.
7 X. Zhong and F. Duan, *Langmuir*, 2015, **31**, 5291-5298.
8 K. Sefiane, *J. Petrol. Sci. Eng.*, 2006, **51**, 238-252.
9 T. Still, P. J. Yunker and A. G. Yodh, *Langmuir*, 2012, **28**, 4984-4988.
10 W. Sempels, R. D. Dier, H. Mizuno, J. Hofkens and J. Vermant, *Nat. Commun.*, 2013, 1-8.
11 X. Zhong and F. Duan, *Soft Matter*, 2016, **12**, 508-513.
12 T. Kajiya, W. Kobayashi, T. Okuzono and M. Doi, *J. Phys. Chem. B*, 2009, **113**, 15460-15466.
13 J. R. Christy, Y. Hamamoto and K. Sefiane, *Phys. Rev. lett.*, 2011, **106**, 205701.
14 X. Zhong and F. Duan, *Euro. Phys. J. E*, 2016, **39**, 1-6.
15 J. R. Christy, K. Sefiane and E. Munro, *J. Bionic. Eng.*, 2010, **7**, 321-328.
16 H. Li, H. Luo, Z. Zhang, Y. Li, B. Xiong, C. Qiao, X. Cao, T. Wang, Y. He and G. Jing, *Phys. Chem. Chem. Phys.*, 2016, **18**, 13018-13025.
17 Chon, C.H.; Paik, S.; Tipton, J.B.; Kihm, K.D. *Langmuir*, 2007, **23**, 2953-2960.
18 Y. Choi, J. Han and C. Kim, *Korean J. Chem. Eng.*, 2011, **28**, 2130-2136.
19 D. Willmer, K. A. Baldwin, C. Kwartnikab and D. J. Fairhurst, *Phys. Chem. Chem. Phys.*, 2010, **12**, 3998-4004.
20 T. S. Wong, T. H. Chen, X. Shen and C. M. Ho, *Anal. Chem.*, 2011, **83**, 1871-1873.

21 P. J. Yunker, T. Still, M. A. Lohr and A. G. Yodh, *Nature*, 2011, **476**, 308-311.
22 M. Anyfantakis, Z. Geng, M. Morel, S. Rudiuk and D. Baigl, *Langmuir*, 2015, **31**, 4113-4120.
23 A. Crivoi and F. Duan, *Phys. Chem. Chem. Phys.*, 2012, **14**, 1449-1454.
24 X. Zhong and F. Duan, *J. Phys. Chem. B*, 2014, **118**, 13636-13645.
25 M. Parsa, S. Harmand, K. Sefiane, M. Bigerelle and R. Deltombe, *Langmuir*, 2015, **31**, 3354-3367.
26 Y. Li, C. Lv, Z. Li, D. Qu*éré* and Q. Zheng, *Soft Matter*, 2015, **11**, 4669-4673.
27 G. J. Dunn, S. K. Wilson, B. R. Duffy, S. David and K. Sefiane, *J. Fluid Mech.*, 2009, **623**, 329-351.
28 Y. Wang, L. Ma, X. Xu and J. Luo, *Soft Matter*, 2015, **11**, 5632-5640.
29 X. Chen, R. Ma, J. Li, C. Hao, W. Guo, B. L. Luk, S. C. Li, S. Yao and Z. Wang *Phys. Rev. Lett.*, 2012, **109**, 116101.
30 A. Sanyal, S. Basu and S. Chaudhuri, *Phys. Chem. Chem. Phys.*, 2016, Accepted Manuscript.
31 A. Miglani and S. Basu, *Soft Matter*, 2015, **11**, 2268-2278.
32 D. Brutin, *Colloids Surf. A Physicochem. Eng. Asp.*, 2013, **429**, 112-120.
33 H. Y. Erbil, *Adv. Colloid Interface Sci.*, 2012, **170**, 67-86.
34 K. Sefiane, S. K. Wilson, S. David, G. J. Dunn and B. R. Duffy, *Phys. Fluids*, 2009, **21**, 062101.
35 W. Ristenpart, P. Kim, C. Domingues, J. Wan and H. Stone, *Phys. Rev. lett.*, 2007, **99**, 234502.
36 X. Xu, J. Luo and D. Guo, *Langmuir*, 2009, **26**, 1918-1922.
37 F. Girard, M. Antoni, and K. Sefiane, *Langmuir*, 2010, **26**, 4576-4580.
38 J. H. Kim, S. B. Park, J. H. Kim and W. C. Zin, *J. Phys. Chem. C*, 2011, **115**, 15375-15383.